

Progress report on testing robustness of the Newton method in data analysis on 2-point correlation function using a MILC HISQ ensemble

Tanmoy Bhattacharya,^a Benjamin J. Choi,^{b,1} Rajan Gupta,^a Yong-Chull Jang,^{c,1} Seungyeob Jwa,^{b,1,*} Sunghee Kim,^{b,1} Sunkyu Lee,^{b,1} Weonjong Lee,^{b,1} Jaehoon Leem,^{d,1} Jeonghwan Pak^{b,1} and Sungwoo Park^{e,1}

^aLos Alamos National Laboratory, MS B285, P.O. Box 1663, Los Alamos, NM 87545-0285, USA

^bLattice Gauge Theory Research Center, CTP, and FPRD, Department of Physics and Astronomy, Seoul National University, Seoul 08826, South Korea

^cPhysics Department, Brookhaven National Lab, Upton, NY 11973, USA

^dComputational Science and Engineering Team, Innovation Center, Samsung Electronics, Hwaseong, Gyeonggi-do 18448, South Korea

^eLawrence Livermore National Lab, 7000 East Ave, Livermore, CA 94550, USA

E-mail: wlee@snu.ac.kr, thoth@snu.ac.kr

We report recent progress in data analysis on the two point correlation functions which will be prerequisite to obtain semileptonic form factors for the $B_{(s)} \rightarrow D_{(s)} \ell \nu$ decays. We use a MILC HISQ ensemble for the measurement. We use the HISQ action for light quarks, and the Oktay-Kronfeld (OK) action for the heavy quarks (b and c). We used a sequential Bayesian method for the data analysis. Here we test the new fitting methodology of Benjamin J. Choi in a completely independent manner.

*The 40th International Symposium on Lattice Field Theory,
July 31-August 4, 2023,
Fermilab, Batavia, Illinois, USA*

¹The SWME collaboration

*Speaker

1. Introduction

Semileptonic form factors for the $B \rightarrow D^{(*)}l\nu$ decays can probe the Cabibbo-Kobayashi-Maskawa (CKM) matrix element $|V_{cb}|$ [1]. This requires the precise data analysis on 2-point correlation functions [2]. Here, we present our recent progress in data analysis on 2-point correlation functions. This work provides an independent cross-checking of the methodology developed by Benjamin Choi in Ref. [3].

We use the MILC HISQ ensembles for the numerical study. In Table 1 (a), we summarize details on the MILC lattice a12m310. For bottom and charm quarks, we use the Oktay-Kronfeld (OK) action [4]. In Table 1 (b), we summarize details on hopping parameters for bottom quarks, and light quark masses.

ID	a (fm)	M_π (MeV)	$L^3 \times T$	κ_{crit}	κ_b	m_l	$N_{\text{cfg}} \times N_{\text{src}}$
a12m310	0.1207(11)	305.3(4)	$24^3 \times 64$	0.051211	0.04102	0.0509	1053×3

(a) Details on the MILC lattice ensemble
(b) Hopping parameters

Table 1: Parameters for the numerical study. Here, N_{cfg} (N_{src}) represents the number of gauge configurations (the number of measurements per gauge configuration).

2. Fit Function

Spectral decomposition of 2-pt correlation functions $C(t)$ measured on the lattice is

$$\begin{aligned}
 C(t) &= \sum_{\tau} \langle \mathcal{O}_{\tau}^{\dagger}(x) \mathcal{O}_{\tau}(0) \rangle \\
 &= \sum_{n=0}^{\infty} (-1)^{n(t+1)} |\langle n | \mathcal{O}(0) | 0 \rangle|^2 \left(e^{-E_n t} + e^{-E_n (T-t)} \right).
 \end{aligned} \tag{1}$$

where the heavy-light meson operator \mathcal{O} is

$$\mathcal{O}_{\tau}(x) \equiv [\bar{\psi}(x) \Gamma \Omega(x)]_{\tau} \chi(x), \tag{2}$$

$$\Gamma = \gamma_5 \quad \text{or} \quad \gamma_j, \tag{3}$$

$$\Omega(x) = \gamma_1^{m_1} \gamma_2^{m_2} \gamma_3^{m_3} \gamma_4^{m_4}, \tag{4}$$

$$x_{\mu} = m_{\mu} a \quad \text{with} \quad m_{\mu} \in \mathbb{Z} \tag{5}$$

with staggered quark field $\chi(x)$, and the ψ is a heavy quark field in the OK action [4]. Here, n is an integer index for energy eigenstates. If n is even (odd), its eigenstate has even (odd) time-parity. The oscillating terms with odd time-parity come from the temporal doubler of staggered quarks [5]. The τ represents taste degrees of freedom for staggered quarks. In our notation, $|0\rangle$ represents not the vacuum state ($|\Omega\rangle$) but the heavy-light meson ground state with energy $E_0 > 0$.

Then, the $n + m$ fitting function [5] is

$$f^{n+m}(t) = g^{n+m}(t) + g^{n+m}(T - t), \tag{6}$$

$$g^{n+m}(t) = A_0 e^{-E_0 t} \left[1 + r_2 e^{-\Delta E_2 t} \times \left(1 + \dots \times (1 + r_{(2n-2)} e^{-\Delta E_{(2n-2)} t}) \dots \right) - (-1)^t r_1 e^{-\Delta E_1 t} \left(1 + \dots \times (1 + r_{(2m-1)} e^{-\Delta E_{(2m-1)} t}) \dots \right) \right] \quad (7)$$

where $r_i = \frac{A_i}{A_{i-2}}$, $\Delta E_i = E_i - E_{i-2}$ for $i \geq 1$ with $E_{-1} = E_0$ and $A_{-1} = A_0$. The $n + m$ fit implies that we include the n even time-parity states and m odd time-parity states in the fitting function.

3. Newton method

When we do the least χ^2 fitting, we use the Broyden-Fletcher-Goldfarb-Shanno (BFGS) algorithm [6–9] to minimize χ^2 . This algorithm belongs to a category of the quasi-Newton method in an optimization problem [10]. The quasi-Newton method requires an initial guess as input to the fitting by construction.

If a initial guess is good, the quasi-Newton method finds the minimum efficiently. If the initial guess is poor (out of radius of convergence), the number of iterations increases and the chance to find the local minima instead of the global minimum grows up. Therefore, it is essential to find a good initial guess close to the true solution (the global minimum), if we want to save computing resources. For this purpose, it is best to obtain initial guess directly from the data, as long as the computing time is negligibly small compared with that of the χ^2 minimizer. It is the multi-dimensional Newton method combined with a scanning method [3] that satisfies these conditions.

The (1-dimensional) Newton method converges quadratically with respect to the distance from the true solution. Hence, it find a root in a few iterations, if the initial guess is sufficiently close to the true solution. However, if the initial guess is sufficiently far away from the true solution, it loses its merit completely. The scanning method converges slowly, but it can narrow down a range to find roots in a few iterations. If we combine the Newton method with the scanning method, it is possible to keep only the merits, while discarding the disadvantages. In other words, the scanning method finds a narrow range to find roots in a few iterations, and then the Newton method can find a root in a few iterations within the narrow range.

Let us consider the 1 + 1 fit as an example. We feed results for the 1 + 0 fit as an initial guess for the A_0, E_0 part of the 1 + 1 fit parameters. In order to obtain initial guess for the remaining parameters r_1 and ΔE_1 , we use the 4-dimensional Newton method combined with the scanning method. The initial range is set to $r_1 \in [0, 1.5]$ and $\Delta E_1 \in [0, 1.0]$ for the scanning method. After a few iterations (1 ~ 2), the scanning method finds such a narrow range for r_1 and ΔE_1 that we may use the Newton method [3] to find an exact solution for Eqs. 8 in a few iterations (7 ~ 10).

The Newton method uses the same time slice combination (*e.g.* $\{t_1 = t_{\min}, t_2, t_3, t_4\}$ for the 1 + 1 fit) as the scanning method. First, we collect all the possible time slice combinations within the fit range ($t_{\min} \leq t \leq t_{\max}$; *e.g.* $t_{\min} = 12$ and $t_{\max} = 26$ for the 1 + 1 fit), before using the scanning and Newton methods. A possible time slice combination should satisfy the following two conditions: 1) it must contains t_{\min} , and 2) the number of even time slices must be equal to that of odd time slices. For each time slice combination, we run the Newton method until we consume all the time slice combinations. If the Newton method find a good solution in a few iterations (7 ~ 10), then we keep it, and if it fails, we discard that time slice combination. The failure rate is about 70% for the 1+1 fit.

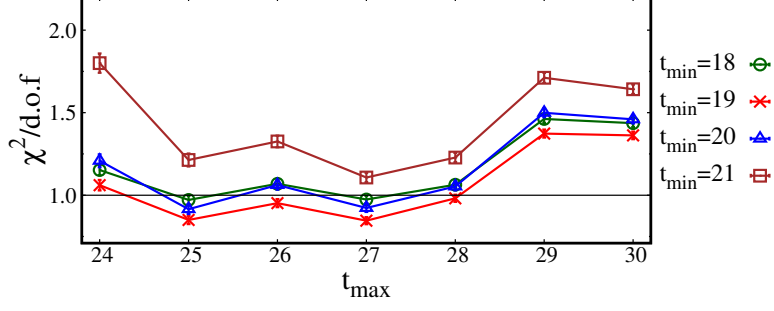


Figure 1: $\chi^2/\text{d.o.f}$ of the 1 + 0 fit as a function of t_{\min} and t_{\max}

The Newton method finds a solution to satisfy the N equations: $q(t_i) = 0$ with $t_i \in \{t_{\min}, t_2, t_3, \dots, t_N\}$, with $N = 2(n + m)$ for the $n + m$ fit (e.g. $N = 4$ for the 1 + 1 fit).

$$q(t_i) = \frac{f(t_i) - C(t_i)}{C(t_i)} = 0. \quad (8)$$

Here, $C(t_i)$ is the 2pt correlator data coming from our numerical measurements, and $f(t)$ is the fitting function in Eq. (6). The stopping condition is

$$\max_{i=1, \dots, N} |q(t_i)| < 10^{-12}. \quad (9)$$

4. Fitting results

Here we describe our sequential Bayesian fitting procedure such as 1+0 fit \rightarrow 1+1 fit \rightarrow 2+1 fit \rightarrow 2+2 fit in detail. We also present results for the $n + m$ fit in each stage of the sequential Bayesian method (SBM). We also explain how to perform stability tests at each stage of the SBM.

4.1 1+0 Fit

Here the fitting function is $f(t) = f^{1+0}(t)$ in Eq. (6). First we do the χ^2 fit for the 1 + 0 fit over the whole appropriate fit ranges. To find initial guess for χ^2 minimizer, we solve the following linear equation:

$$\begin{bmatrix} \sum_i \frac{C^2(t_i)}{\sigma^2(t_i)} & \sum_i t_i \frac{C^2(t_i)}{\sigma^2(t_i)} \\ \sum_i t_i \frac{C^2(t_i)}{\sigma^2(t_i)} & \sum_i t_i^2 \frac{C^2(t_i)}{\sigma^2(t_i)} \end{bmatrix} \begin{bmatrix} \ln A_0^{\text{ig}} \\ -E_0^{\text{ig}} \end{bmatrix} = \begin{bmatrix} \sum_i \frac{C^2(t_i)}{\sigma^2(t_i)} \ln |C(t_i)| \\ \sum_i t_i \frac{C^2(t_i)}{\sigma^2(t_i)} \ln |C(t_i)| \end{bmatrix}, \quad (10)$$

which assumes the diagonal approximation in the covariance matrix [11]. Here $A_0^{\text{ig}}, E_0^{\text{ig}}$ denote the initial guesses, and $\sigma(t_i) = \sqrt{V(t_i, t_i)}$, where $V(t_i, t_i)$ is the covariance matrix of the data $C(t_i)$. Here the summation \sum_i is over the fit range: $t_{\min} \leq t_i \leq t_{\max}$. The optimal fit range for the 1+1 fit is determined by the minimum of χ^2/dof . In Fig. 1 we present results for χ^2/dof as a function of t_{\min} and t_{\max} . We find that the optimal fit range is $19 \leq t \leq 28$: $t_{\min} = 19$ and $t_{\max} = 28$. Note that $t_{\max} = 28$ is fixed for the remaining fits of the SBM.

Let us define the Newton mass $m_{\text{newt}}^d(t) = E_0(t)$ at zero momentum projection. At each time slice t , we obtain $m_{\text{newt}}^d(t)$ by solving two equations: $q(t) = q(t + d) = 0$, using the 2-dimensional

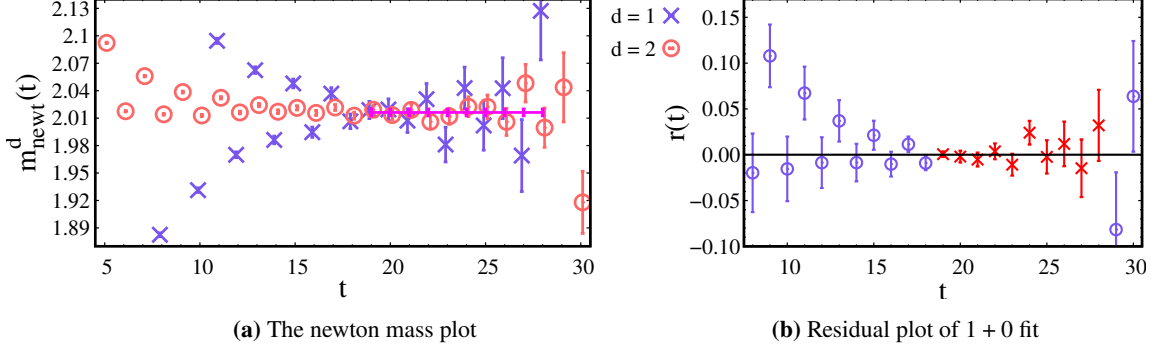


Figure 2: Results of 1 + 0 fit

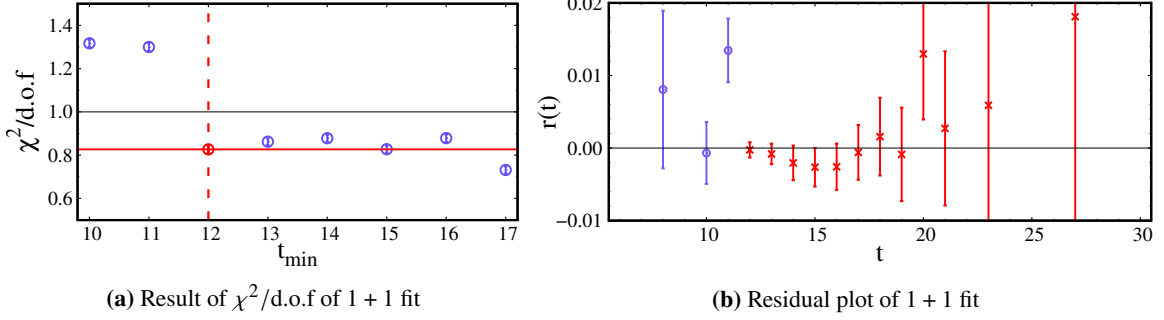


Figure 3: Results of 1 + 1 fit

Newton method. We use the least χ^2 fitting results for A_0 and E_0 as initial guess for the 2-d. Newton method. In Fig. (2a), we present results for $m_{\text{newt}}^d(t)$ with $d = 1$ and $d = 2$ as a function of time t .

Results for the 1+0 fit are summarized in Table (2). In order to check the quality of fitting, we plot the residual, $r(t) = \frac{C(t) - f(t)}{|C(t)|}$ in Fig. 2 (b). Here the red (blue) symbols represent the residual within (out of) the fit range.

Fit range	A_0	E_0	$\chi^2/d.o.f.$	p -value
[19, 28]	0.01735(125)	2.0162(38)	0.981(22)	0.448(17)

Table 2: Result of the 1 + 0 fit

4.2 1+1 Fit

We use results of the 1+0 fit to determine Bayesian priors for the 1+1 fit. We set the Bayesian prior widths (BPW) to the maximum fluctuation (σ_p^{mf}) or the signal cut (σ_p^{sc}) of the A_0 and E_0 parameters.¹ We choose $\min(\sigma_p^{mf}, \sigma_p^{sc})$ for the BPW.

Starting from $t_{\text{min}}^{1+1} = t_{\text{min}}^{1+0} - 2$, we run t_{min}^{1+1} over the lower values until χ^2/dof overflows the appropriate criterion. In Fig. 3 (a) we present χ^2/dof as a function of t_{min}^{1+1} . Here we find that the optimal fit range is $t_{\text{min}}^{1+1} = 12$. In Fig. 3 (b) we present the residual $r(t)$ with the fit range $12 \leq t \leq 28$. The 1+1 fit results are summarized in Table 3.

¹The signal cut means that the error (= noise) is the same as the average (= signal), when the parameters should be positive thanks to physical reasons.

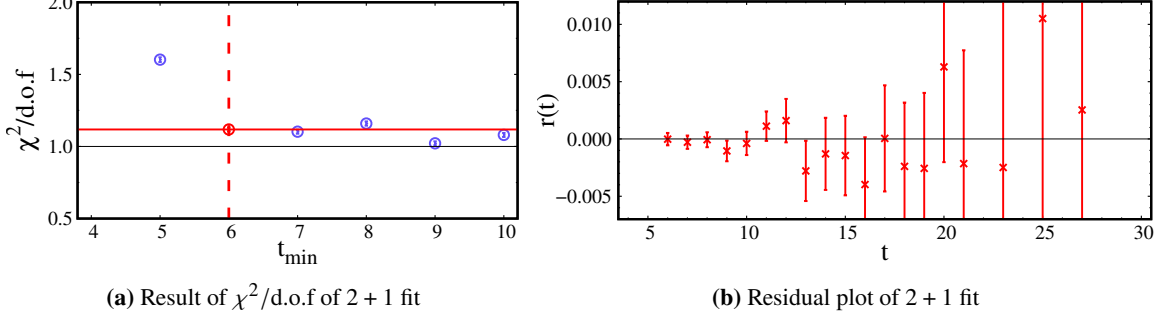


Figure 4: Results of 2 + 1 fit

4.3 2+1 Fit

First, we use the results of 1 + 1 to set the BPW for 2 + 1 fit. Starting from $t_{\min}^{2+1} = t_{\min}^{1+1} - 2$, we run t_{\min}^{2+1} over the lower values until χ^2/dof overflows the criterion. In Fig. 4 (a) we present χ^2/dof as a function of t_{\min}^{2+1} . Here we find that $t_{\min}^{2+1} = 6$ is the optimal fit range for the 2+1 fit. In Fig. 4 (b) we present the residual $r(t)$ with the fit range $6 \leq t \leq 28$.

Once we choose the fit range, we can perform the stability tests to find the optimal prior widths for A_0 and E_0 , which minimize prior widths with no change in fit results. Here we adopt the same notation and convention as in Ref. [12]. First, we first do the fit with maximum prior widths: $\sigma_p^{\max}(A_0) = \sigma_p^{\text{sc}}$, and $\sigma_p^{\max}(E_0) = \sigma_p^{\text{mf}}$, which correspond to the blue circles in Fig. 5. Here note that $\sigma_{\max}^{A_0} = \sigma(A_0; \sigma_p^{\max}(A_0), \sigma_p^{\max}(E_0))$ and $\sigma_{\max}^{E_0} = \sigma(E_0; \sigma_p^{\max}(A_0), \sigma_p^{\max}(E_0))$. The units for x -axis are $[\sigma_{\max}^{A_0}] = 5.54 \times 10^{-4}$, and $[\sigma_{\max}^{E_0}] = 2.01 \times 10^{-3}$. We find the optimal prior widths (the red square symbols, $\sigma_p^{\text{opt}}(A_0 \text{ or } E_0)$) such that they are the minimum prior widths which does not disturb the fit results obtained with the maximum prior widths. Here the σ_σ (blue dashed lines) represents the error of the error.

Results of the 2+1 fit are summarized in Table 4.

4.4 2+2 Fit

For the 2+2 fit we set the prior widths as follows.

1. [A_0 and E_0] We use the results of the stability tests for the 2+1 fit as the prior widths for A_0 and E_0 .
2. [R_1 and ΔE_1] We set the prior widths to the signal cuts for both.
3. [R_2 and ΔE_2] We set the prior widths to the signal cuts for both.
4. [R_3 and ΔE_3] No prior information.

t_{\min}	A_0 (10^{-2})	E_0	r_1	ΔE_1	$\frac{\chi^2}{\text{d.o.f.}}$
prior	1.735(1735)	2.0162(538)			
12	1.847(31)	2.0198(13)	0.28(14)	0.193(39)	0.827(15)

Table 3: Result of the 1 + 1 fit

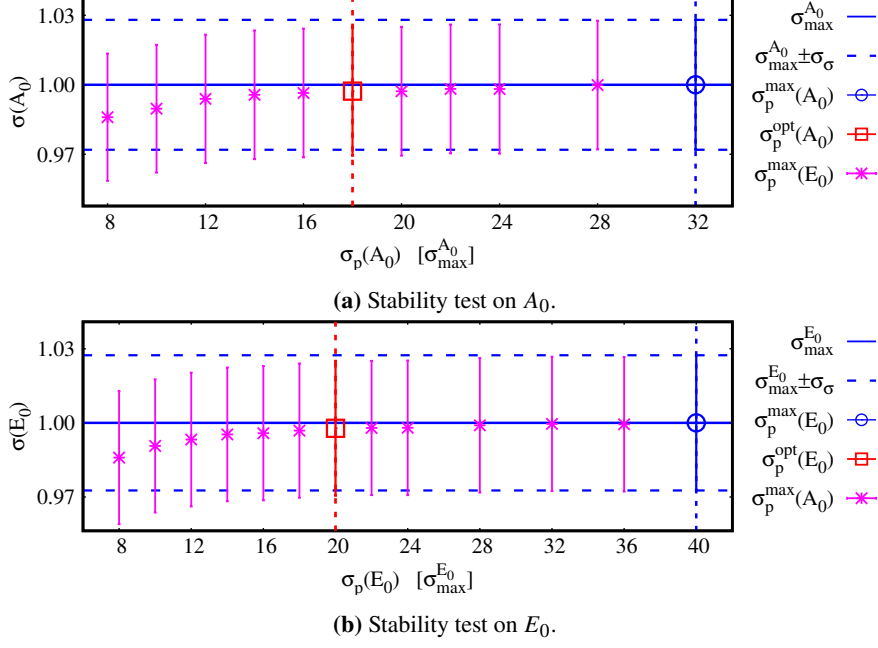


Figure 5: Results of the stability test for the 2 + 1 fit.

t_{\min}	A_0 (10^{-2})	E_0	r_1	ΔE_1	r_2	ΔE_2	$\frac{\chi^2}{\text{d.o.f.}}$
prior	1.789(997)	2.0180(400)	0.69(69)	0.257(257)			
6	1.789(55)	2.0180(20)	0.69(3)	0.257(6)	1.04(20)	0.372(60)	1.011(14)

Table 4: Result of the 2 + 1 fit

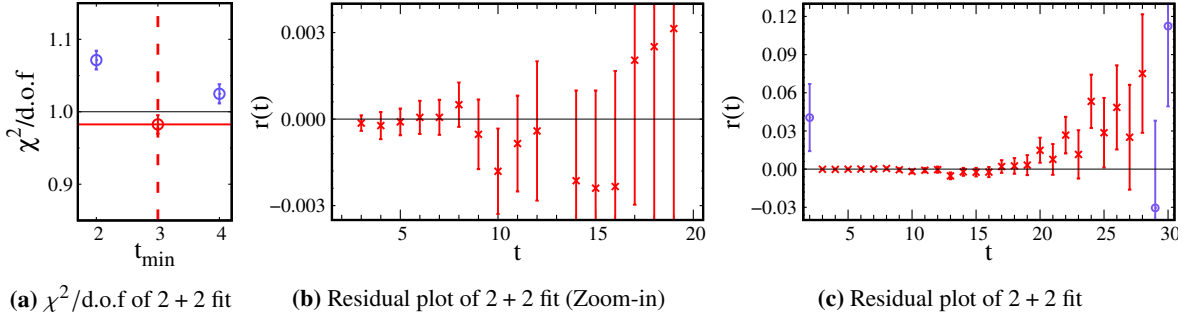


Figure 6: Results of 2 + 2 fit

Starting from $t_{\min}^{2+2} = t_{\min}^{2+1} - 2 = 4$, we run t_{\min}^{2+2} over the lower values. In Fig. 6 (a) we present χ^2/dof as a function of t_{\min}^{2+2} . The physical positivity [13] constrains t_{\min} such that $t_{\min} \geq 3$. Here we find that $t_{\min}^{2+2} = 3$ is the optimal fit range. In Fig. 6 (c) we present the residual $r(t)$ with the fit range $3 \leq t \leq 28$.

Once we choose the fit range, we do the stability tests to find the optimal prior widths for r_1 and ΔE_1 . First, we first do the fit with maximum prior widths: $\sigma_p^{\max}(r_1)$, and $\sigma_p^{\max}(\Delta E_1)$, which correspond to the blue circles in Fig. 7. Here note that $\sigma_{\max}^{r_1} = \sigma(r_1; \sigma_p^{\max}(r_1), \sigma_p^{\max}(\Delta E_1))$ and $\sigma_{\max}^{\Delta E_1} = \sigma(\Delta E_1; \sigma_p^{\max}(r_1), \sigma_p^{\max}(\Delta E_1))$, while $\sigma_p^{\max}(r_1) = \sigma_p^{\text{sc}}(r_1)$ and $\sigma_p^{\max}(\Delta E_1) = \sigma_p^{\text{sc}}(\Delta E_1)$.

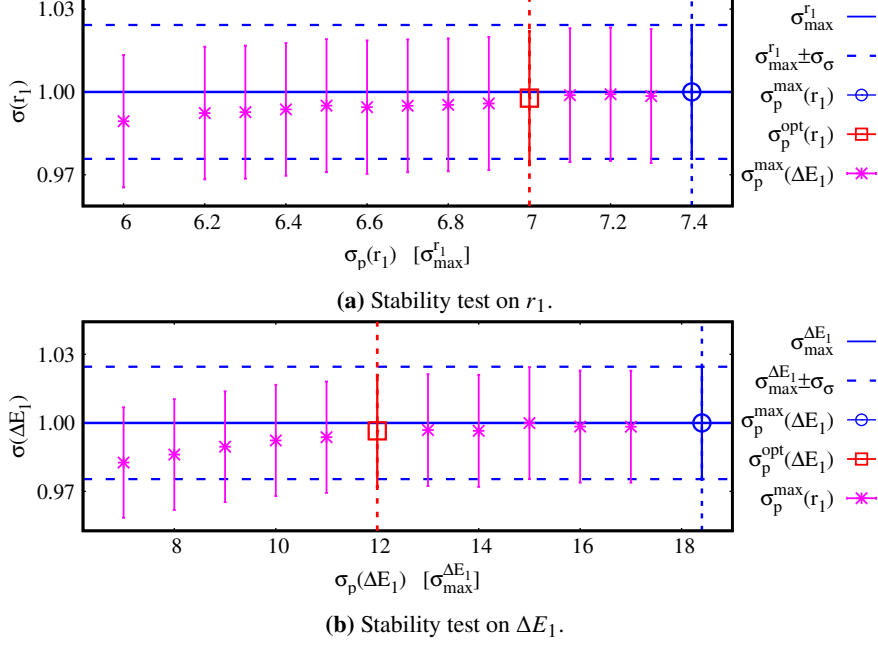


Figure 7: Results for the stability test in the 2 + 2 fit.

The units for x -axis are $[\sigma_{\max}^{r_1}] = 7.8 \times 10^{-2}$, and $[\sigma_{\max}^{\Delta E_1}] = 1.31 \times 10^{-2}$. In Fig. 7 the red square symbols represent the optimal prior widths, $\sigma_p^{\text{opt}}(r_1 \text{ or } \Delta E_1)$.

Results of the 2+2 fit are summarized in Table 5.

t_{\min}	$A_0 (10^{-2})$	E_0	r_1	ΔE_1	
prior	1.858(997)	2.0203(400)	0.58(53)	0.242(171)	
3	1.858(24)	2.0203(11)	0.58(8)	0.242(13)	
	r_2	ΔE_2	r_3	ΔE_3	$\frac{\chi^2}{\text{d.o.f.}}$
prior	1.91(191)	0.512(512)			
3	1.91(6)	0.512(17)	1.63(19)	0.480(114)	0.983(13)

Table 5: Result of the 2 + 2 fit.

Acknowledgments

We would like to thank A. Kronfeld, and C. Detar for helpful discussion on fitting. We thank the MILC collaboration and Chulwoo Jung for providing the HISQ lattice ensembles. The research of W. Lee is supported by the Mid-Career Research Program (Grant No. NRF-2019R1A2C2085685) of the NRF grant funded by the Korean government (MSIT). W. Lee would like to acknowledge the support from the KISTI supercomputing center through the strategic support program for the supercomputing application research (No. KSC-2018-CHA-0043, KSC-2020-CHA-0001, KSC-2023-CHA-0010). Computations were carried out in part on the DAVID cluster at Seoul National University.

References

- [1] **HFLAV** Collaboration, Y. Amhis *et al.*, *Averages of b -hadron, c -hadron, and τ -lepton properties as of 2021*, [2206.07501](#).
- [2] **Fermilab Lattice, MILC** Collaboration, J. A. Bailey *et al.*, *Update of $|V_{cb}|$ from the $\bar{B} \rightarrow D^* \ell \bar{\nu}$ form factor at zero recoil with three-flavor lattice QCD*, *Phys. Rev. D* **89** (2014), no. 11 114504, [[1403.0635](#)].
- [3] T. Bhattacharya, B. J. Choi, R. Gupta, Y.-C. Jang, S. Jwa, S. Lee, W. Lee, J. Leem, S. Park, and B. Yoon, *Improved data analysis on two-point correlation function with sequential Bayesian method*, *PoS LATTICE2021* (2021) 136, [[2204.05848](#)].
- [4] M. B. Oktay and A. S. Kronfeld, *New lattice action for heavy quarks*, *Phys. Rev. D* **78** (2008) 014504, [[0803.0523](#)].
- [5] M. Wingate, J. Shigemitsu, C. T. H. Davies, G. P. Lepage, and H. D. Trottier, *Heavy light mesons with staggered light quarks*, *Phys. Rev. D* **67** (2003) 054505, [[hep-lat/0211014](#)].
- [6] C. G. BROYDEN, *The Convergence of a Class of Double-rank Minimization Algorithms I. General Considerations*, *IMA Journal of Applied Mathematics* **6** (03, 1970) 76–90, [<https://academic.oup.com/imamat/article-pdf/6/1/76/2233756/6-1-76.pdf>].
- [7] R. Fletcher, *A new approach to variable metric algorithms*, *The Computer Journal* **13** (01, 1970) 317–322, [<https://academic.oup.com/comjnl/article-pdf/13/3/317/988678/130317.pdf>].
- [8] D. Goldfarb, *A family of variable-metric methods derived by variational means*, *Mathematics of Computation* **24** (1970) 23–26.
- [9] D. F. Shanno, *Conditioning of quasi-newton methods for function minimization*, *Mathematics of computation* **24** (1970), no. 111 647–656.
- [10] R. Fletcher, *Newton-Like Methods*, ch. 3, pp. 44–79. John Wiley & Sons, Ltd, 2000. <https://onlinelibrary.wiley.com/doi/pdf/10.1002/9781118723203.ch3>.
- [11] C. Michael, *Fitting correlated data*, *Phys. Rev. D* **49** (Mar, 1994) 2616–2619.
- [12] T. Bhattacharya, B. J. Choi, R. Gupta, Y.-C. Jang, S. Jwa, S. Lee, W. Lee, J. Leem, and S. Park, *Current progress on the semileptonic form factors for $B \rightarrow D^{(*)} l \nu$ decay using the Oktay-Kronfeld action*, *PoS LATTICE2023* (2023).
- [13] M. Luscher and P. Weisz, *Definition and General Properties of the Transfer Matrix in Continuum Limit Improved Lattice Gauge Theories*, *Nucl. Phys. B* **240** (1984) 349–361.